ELSEVIER

Chemical Engineering Journal 77 (2000) 119–125

Chemical Engineering Journal

www.elsevier.com/locate/cej

Status and applications of microelectrical resistance tomography ☆

H.S. Tapp *, R.A. Williams

Department of Mining and Mineral Engineering, University of Leeds, Leeds, LS2 9JT, UK

Abstract

Electrical resistance tomography (ERT) is part of a suite of real-time low-cost two-dimensional imaging techniques which exploit the differences in the electrical properties of, for example, several flowing particulate systems. A physical sensor typically comprises an annular array of 16 electrodes mounted on a pipe wall such that the electrodes make electrical contact with the measured medium. Although the image fidelity is currently poor compared to X-ray tomography, the sensors can be scaled to suit the application. A microelectric resistance sensory system (MERT) is being developed for on-line interrogating down to 20–1000 μm length scales.

This paper reviews the development of microelectrical sensing systems and reconstruction and interpretation methods using as example, a feasibility study on a 56 mm diameter bore sensor. This illustrates the limitations in the widely employed procedure of employing generic tomographic sensors and image feature extraction methods to extract application specific control parameters.

Keywords: Microelectrical resistance tomography; Characterisation; Particle and colloid suspensions; Emulsions and pastes

1. Introduction

Electrical resistance tomography (ERT) belongs to a group of imaging methods collectively termed as electrical tomography techniques, that have been extensively reviewed [1–4]. These methods exploit differences in the electrical properties of different materials, or process-related state changes to provide slice-images of the measurand under scrutiny. Benefits of these sensors are their relative low-cost, fast image rates and that the size of the sensors can readily be tailored to suite the scale of the application. The task of image reconstruction from electrical measurements, typically acquired from circular single- or multi-plane transducer arrays, is considerable resulting in a subsequent compromised image quality. This is due to the nature of the interaction between the electromagnetic field and the measurand, and physical restraints on the number of transducers and hence permitted independent measurements. An image resolution in the order of 10% of the bore diameter is typically quoted. The characterisation of flowing particulate systems such as suspended processed minerals, emulsions and pastes subsequently require ERT sensors with a bore diameter of the order of a few millimetres. Our aim is to construct sensors with a bore diameter of the order of 1 mm, however, during sensor development larger scale systems have been constructed. The following adjectives will be used to differentiate the different scales of the sensor bore diameter: macro (>10 mm), meso (1–10 mm) and micro (<1 mm).

An example of an electrical particle characterisation instrument is the Coulter Counter (http://www.beckmancoulter.com/). This device consists of an outer and inner chamber connected by a small aperture. In each chamber a large electrode is immersed in a conducting solution. The aperture restricts the flow of electrical current between the two electrodes. Particles are drawn through the aperture resulting in pulsed fluctuations in the impedance, with the height of the pulse being proportional to the volume of electrolyte displaced. The Coulter Counter is thus able to both count and provide size (volume) distribution information. Merits of this technique include speed (approximately 8000 particles/s) and simplicity of design and operation. In addition the technique is insensitive to the position of the particle within the sensing space (aperture) thus overcoming a fundamental complexity experienced by ERT sensors.

Advances in silicon fabrication technology have resulted in the development of on-chip bio-medical electrical sensors. Recently, reported work includes the development at Bangor (http://www.sees.bangor.ac.uk/~rslee/biochip/) of biological cell manipulation and identification techniques using, for example, travelling wave dielectrophoresis and electrorotation [5–9]. Other developments include work carried out at Nanogen (http://www.nanogen.com/) in San Diego on the

☆ Presented at the 1st World Congress on Industrial Process Tomography, 14–17 April 1999, Buxton, Derbyshire.

* Corresponding author. Tel.: +44-113-233-2392; fax: +44-113-233-2781.
E-mail address: h.s.tapp@leeds.ac.uk (H.S. Tapp).

1385-8947/00/$ – see front matter
PII: S1385-8947(99)00145-X

charge labelling of a mixture of human blood cells and *Escherichia coli* [10]. The charge labels permit the separation of the *E. coli* that are then lysed using high voltage pulses.

Advances in silicon fabrication technology have also resulted in the development of application specific integrated circuits (ASICs), in which the measurement electronics of the data acquisition system (DAS) are closely associated with the tomographic transducers [11]. This work is particularly germane since it has been developed for use with a micro (1 mm bore diameter) electrical capacitance tomography system.

The following account of work related to various aspects of the development of miniaturised ERT sensors is presented in two sections, based on the geometry of the sensor: axially extended electrodes or point electrodes. The axially extended electrode sensors consist of wire electrodes that lie flush with the vessel wall. The majority of the first section contains an account of a phantom evaluation of a macroscale axially extended electrode sensor.

2. Axially extended electrode systems

A mesoscale ERT sensor has been developed to investigate changes in the radial distribution of particulate solids with flow regime [12,13]. The sensor comprised 16 mm × 8 mm long (0.3 mm diameter) silver wire electrodes lying flush with a 6 mm diameter bore (Fig. 1a).

The authors have characterised a macroscale sensor using rod and sphere phantoms. The wire sensor, depicted in Fig. 1b, comprised 16 mm × 62 mm long stainless steel wire electrodes mounted parallel to the axis, and flush with the internal wall of a 56 mm internal diameter Perspex pipe. The sensor was connected to an ITS Prototype 1000 [14] (http://www.itoms.com/) data acquisition system (DAS). This operates at 9.6 kHz and employs the adjacent measurement protocol [2] to yield a total of 104 potential difference measurements. Each recorded measurement represented the mean of eight samples. The DAS was connected to a Gateway 2000 personal computer via a nine-pin RS232 serial communication port.

The purpose of the rod phantom experiments was to conduct a quantitative comparison of estimates of the size and position of various phantoms based on the results obtained from three different reconstruction techniques. This feasibility study also aims to illustrate the difficulties in extracting summary information from reconstructed tomographic images. Rods were chosen since they maintain a uniform cross-section throughout the (axially extended) measurement space. The spherical phantom experiments were conducted to mimic the passage of a single particle through the ERT sensor and hence gain some insight into the images that might be obtained from a single plane micro-ERT sensor.

A Perspex 5 mm thick template was affixed to the top of the sensor. Into the template were drilled 20 8 mm holes, evenly positioned throughout the cross-sectional area of the sensor. The template allowed the reproducible positioning of either single- or dual-8 mm diameter rod phantoms. Both conducting (stainless steel) and non-conducting (glass) rod phantoms were employed. The sensor was filled with 0.005 M KCl saline solution, which corresponds to a conductivity of 0.65 mS. With the template removed, a further experiment was performed using a 25 mm spherical non-conducting (ceramic) phantom, suspended into the saline by thread and positioned coaxial to that of the sensor. The phantom was lowed in 1 cm increments past the electrodes over a total distance of 15 cm.

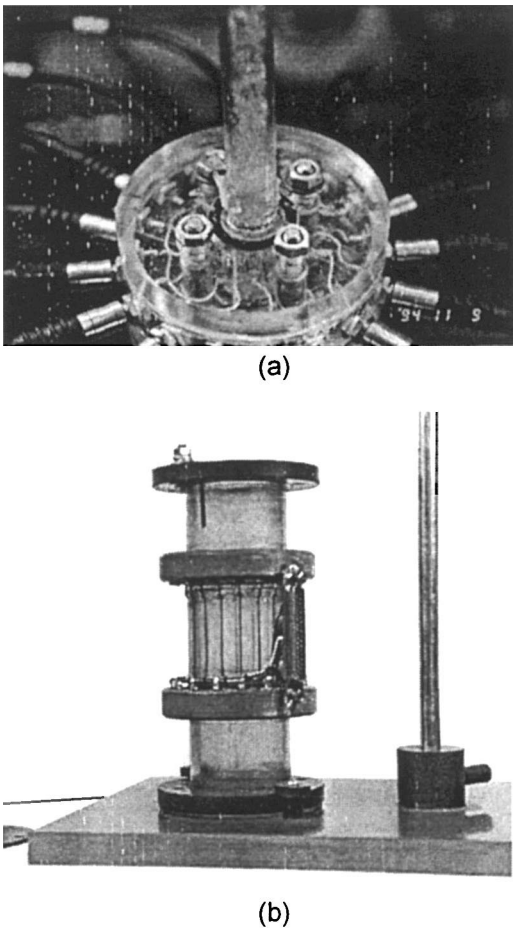

Fig. 1. (a) Mesoscale sensor with axially extended electrodes after [13]. (b) The macroscale sensor used in the rod and sphere phantom evaluation.

One hundred sets of measurements were recorded with the sensor initially containing saline only, to provide a reference, and for each phantom position. A two-thirds trimmed mean was computed for each set of 100 measurements, which were used in the subsequent image reconstruction analysis.

Image analysis was performed on the estimates obtained using three reconstruction techniques: linear back projection (LBP), a modified Newton–Raphson method (MNR) and a parametric model based technique (PM). The algorithms employ a single point calibration based on a set of reference voltages acquired with the sensor filled only with a solution of known conductivity. Nine case examples of the

8 mm rod experiments are used in this comparison comprising three positions of a single glass rod phantom, three of a single metal rod, and three dual-rod phantoms: glass–glass, steel–steel and glass–steel.

The *linear back projection* (LBP) algorithm evaluated is a variant of the scheme originally proposed by Barber and Brown [15]. The conductivity distribution is assumed to comprise a number of discrete regions within the measurement space such that the conductivity within each region is constant. The estimated conductivity distribution (image) is represented using 316 square pixels of equal area, which fill the cross-sectional area of the sensor. An example of the image obtained is presented in Fig. 2a.

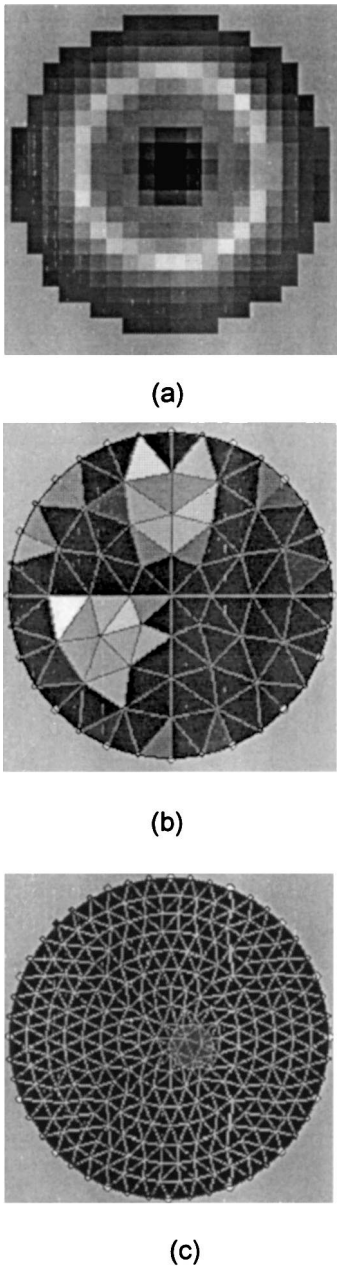

Fig. 2. Images of single glass rod, dual glass rods and single steel rod reconstructed using (a) LBP, (b) MNR and (c) PM, respectively.

Once the conductivity distribution has been estimated, further analysis is required to extract salient features from the image. Two descriptive parameters were chosen: the area and distance of the rod or rods, relative to the sensor dimensions. The criterion for assigning a pixel occupied by a rod was based on the following analysis. One hundred successive measurements were recorded with the sensor filled only with 0.005 M KCl saline solution. These were then converted into corresponding images using LBP. Fluctuations in these voltage measurements were assumed to arise solely from instrumental sources. The standard deviation in the value of each of the 316 pixels was used as a measure of the variation experienced over the 100 samples. The greatest standard deviation, slightly larger than 0.01 mS, was obtained for pixels close to the sensor wall (Fig. 3).

It was considered that any pixel that deviated by greater than 10 times that amount could be attributed to arising from the presence of the phantom. Since the experiments were performed using a saline solution with conductivity 0.65 mS, this corresponded to upper and lower threshold values of 0.75 and 0.55 mS, respectively. Accordingly, the number of pixels lying outside of the region bounded by these threshold values was taken as an estimate of the area of the rod or rods. Division by the total number of pixels (316) thus yielded an estimate of the phantom area relative to the cross-sectional area of the sensor. The diameter of the sensor and rods used throughout were 56 and 8 mm, respectively. A rod therefore had a nominal relative cross-sectional area of 0.02. In practice this criteria was sufficient to always correctly determine the presence of the phantoms.

The co-ordinates of the rod centre (X, Y) were calculated using the following weighted summations

$$X = \frac{\sum w_i x_i}{\sum w_i}, \qquad Y = \frac{\sum w_i y_i}{\sum w_i}, \quad w_i = |p_i - 0.65| \quad (1)$$

where p_i refers to the pixel value with co-ordinates (x_i, y_i) which meets either the lower or upper threshold criteria. Separate calculations were performed to identify all the pixels with values that met the lower threshold criteria, or all those that met the upper threshold criteria. Note that pixel values having greater absolute differences in estimated

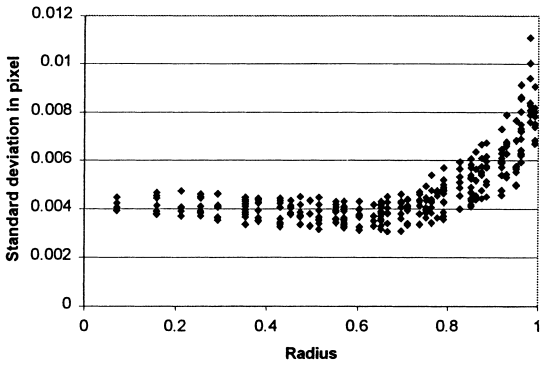

Fig. 3. Error variation with radius.

conductivity (with respect to the assumed saline conductivity, 0.65 mS) are permitted to assert a greater influence on the calculated position of the rod centre. This approach was preferred over one in which pixel values meeting the threshold criteria are truncated to the threshold value, giving them equal influence over the determination of the rod centre.

In the dual glass rod example, the rods were separated sufficiently to permit estimates of the positions of the rods by restricting the regions over which the weighted summation was performed (by inspection) to coincide with those at which each rod was known to lie. This manual procedure could be automated if many images of this nature required analysis. In the dual steel rod example, the rods were positioned sufficiently close to each other for them not to be resolved by any of the reconstruction algorithms evaluated.

The *modified Newton–Raphson* (MNR) algorithm is based on an Abdullah et al. [16] implementation of a scheme first described by Yorkey. This algorithm was the most computational intensive of the three used. The conductivity distribution is assumed to comprise a number of discrete regions within the measurement space such that the conductivity within each region is assumed constant. The estimated conductivity distribution (image) is represented using 104 triangular regions of equal area, which fill the cross-sectional area of the sensor. An example of such an image is presented in Fig. 2b. The procedure requires sufficient regularisation to prevent solution divergence. Subsequently a Tikhonov–Marquardt constraining coefficient of 0.9 was used throughout. This gain in stability was at the expense of the convergence rate and subsequently 512 iterations were performed, by which point the solution was assumed to have converged.

The *parametric model* (PM) algorithm evaluated was developed for the analysis of ERT data collected by a sensor comprising eight planes of 16 electrodes, integrated into the conical section of a solid–liquid cyclonic separator [17]. The algorithm outputs the angular position and radius (relative to the sensor dimensions) of a single circular object of known conductivity. This procedure is clearly also relevant to this particular project as it enables the direct determination of the size and position relative to the sensor dimensions of rod phantoms (or particles). An example of the image produced by this method is displayed in Fig. 2c. Note that other parametric model based reconstruction schemes for electrical tomography have been proposed elsewhere [18–20].

The PM scheme may be compared with the LBP and MNR routines described previously. Both of these are examples of generic reconstruction algorithms. For a given set of measurements (and reference) both will produce estimate conductivity variations, and so can (and have) been employed for studying a broad range of applications. Compare this with the parametric model that has been developed specifically to estimate the size and position of a single circular target. For this reconstruction algorithm the extraction of the area and position of the rod (or rods) relative to the sensor dimensions becomes simple as they are estimated directly.

Table 1
Comparison of estimated and actual relative position and area of single- or dual-rod phantoms

Phantom	Radial distance				Area			
	LBP	MNR	PM	Actual	LBP	MNR	PM	Actual
Glass	0.00	0.01	0.07	0.00	0.02	0.13	0.02	0.02
Glass	0.01	0.09	0.44	0.48	0.05	0.11	0.02	0.02
Glass	0.13	0.27	0.65	0.76	0.12	0.10	0.02	0.02
Metal	0.00	0.08	0.15	0.00	0.10	0.13	0.02	0.02
Metal	0.17	0.28	0.52	0.48	0.27	0.22	0.04	0.02
Metal	0.27	0.53	0.56	0.76	0.27	0.20	0.04	0.02
Glass 1	0.48	0.50	0.54	0.48	0.06	0.08	0.01	0.02
Glass 2	0.56	0.56	0.47	0.48	0.14	0.09	0.01	0.02
Glass	0.04	0.13	0.69	0.76	0.07	0.13	0.01	0.02
Metal	0.00	0.07	0.16	0.48	0.02	0.23	0.01	0.02
2 × Metal	0.29	0.36	0.28	0.61	0.42	0.24	0.06	0.04

The *results of the image analysis* are presented in Table 1. Consider first the predicted radial position of the rods. There was close agreement between the three estimates, and actual position of the centrally positioned glass rod with the order of closest agreement to the actual position being as follows: LBP, MNR and PM. As the position of the rod from the centre of the sensor is increased, all three techniques showed a tendency to underestimate the distance from centre with the order of closest agreement to the actual position being as follows: PM, MNR, and LBP. These trends are also exhibited in the single metal rod, the dual glass metal rod, and dual metal rod cases, while none of the techniques were able to resolve the positions of the two metal rods. Interestingly, all three techniques estimation of the position of the dual glass rod case was in close agreement to the actual positions of the rods.

Considering the estimated area of the rods, the following trends were observed. The PM correctly estimated the area of the single glass rod, at each of the rod positions. The MNR consistently underestimated the area of the glass, and exhibited a slight trend to increase the underestimation as the position of the rod from the centre increased. The LBP correctly estimated the area of the centrally positioned glass rod but then exhibited a pronounced trend to overestimate the area as the position of the rod from centre increased. For the centrally positioned single metal rod the PM correctly estimated the area of the rod, while the MNR and LBP methods both underestimated the rod area. These techniques, however, produced area estimates for the other two (metal rod) cases that were in close agreement with the actual area. For these cases the PM consistently overestimated the area by a factor of 2. In the dual glass rod and dual glass metal cases the PM consistently underestimated the rod area by a factor of 2, while LBP and MNR both markedly overestimated the rod's area by varying amounts. The greatest overestimation was the MNR prediction of the metal rod in the dual metal–glass rod case. This was over 11 times the actual area. The greatest overestimation by LBP was a by a factor of 7, found in the determination of one of the glass

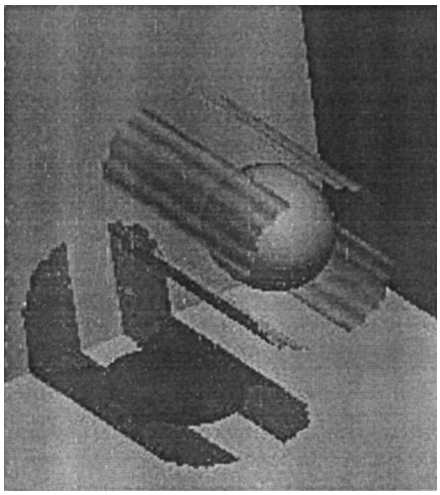

Fig. 4. LBP images of ceramic spherical phantom presented as pseudo three-dimensional iso-contour plot.

rods from the dual glass rod example. For the dual metal rod case LBP produced the closest agreement to the actual area with MNR and PM underestimating and overestimating the area, respectively.

A graphical visualisation of the images obtained using LBP on the ceramic spherical phantom data is shown in Fig. 4. The individual images were stacked and then converted into a pseudo three-dimensional iso-surface conductivity plot. At this stage, the aim was not to perform any quantitative analysis on the spherical phantom data. The figure does, however, provide a fascinating glimpse of the future potential of MERT to characterise flowing particulate systems.

From the data presented, it has been shown that predictions by three tomographic reconstruction techniques of the position and area of the test rod phantoms exhibited a complex dependency with rod position. The basis by which these estimates were derived varied considerably, as did the effort required producing the images and extracting the salient information.

There has been reported the construction and preliminary data obtained from a printed circuit board (PCB) based MERT sensor [21]. The sensor comprised 16 (60 μm diameter) gold wire electrodes equi-spaced around a 0.9 mm diameter bore. The sensor was connected to a DAS operating at 82 kHz yielding static images of conducting (copper wire) and non-conducting (human hair) rod phantoms, and dynamic images of glass microspheres.

3. Point electrode systems

Previous work on fabricating miniaturised ERT sensors includes proposed manufacturing schemes at the mesoscale [22]. Two methods were advocated. One method consisted of drilling 16 equi-spaced holes into a 5 cm diameter tube. Platinum wire was then inserted through opposing holes prior to embedding in an epoxy resin matrix. Once cured, a 10 mm diameter hole is drilled through the centre to form the sensor bore. The alternative proposed sensor fabrication protocol again involved drilling 16 equi-spaced hole through a 5 cm diameter tube to accept platinum wire. A centrally positioned pin enabled the wire to be wound such that it entered and left from adjacent holes. The tube was then filled with epoxy, which once cured accepted a 10 mm diameter drilled hole. Subsequent extensive phantom evaluation of sensors with diameters in the range 13–150 mm has also been reported [23].

The construction of a 1 mm bore diameter PCB based ERT sensor has been reported (Fig. 5) [24]. The sensor comprised 16 equi-spaced gold coated electrodes surrounding the 1 mm diameter bore. Each electrode had dimensions 100 μm × 380 μm. Fig. 5 shows a single PCB sensor (a), a sensor unit comprising a stack of four planes (b), and this unit integrated into a bench-top emulsion flow rig (c).

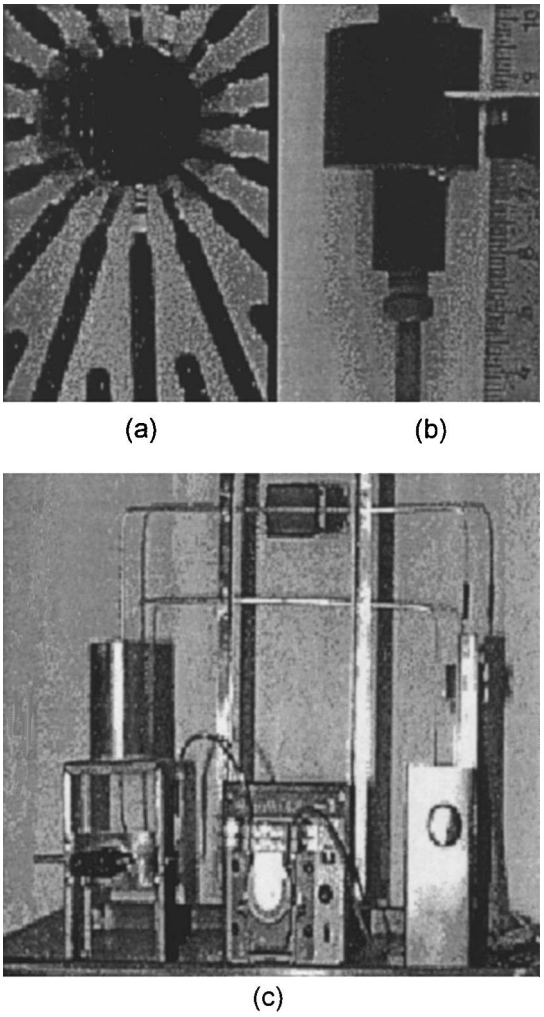

Fig. 5. (a) Detailed view of a 1 mm diameter bore PCB sensor. (b) A sensor unit comprising four planes of PCB sensors. (c) A bench-top emulsion flow rig incorporating the four plane PCB sensor unit.

Further information relating to fabrication method, characterisation, and integration into a process pipe are discussed elsewhere [25].

In addition to the design of the PCB sensor, analytical methods suitable for processing ERT measurements on emulsions and pastes were described. Much of the suggested analysis centred on pixel-based feature extraction. For example, it was suggested that if MERT were to be applied to relatively dilute oil/water emulsions, a series of sequentially obtained tomographic images from a single plane ERT sensor could be stacked to produce a pseudo three-dimensional resistivity map [24]. By using image manipulation software to present the data as an iso-conductivity plot salient features relating to the emulsion morphology could be visualised. The method was illustrated using simulated data of ERT measurements on either a coalesced or uncoalesced 10% oil in water.

It was proposed that this method could be extended to treat more concentrated emulsions and pastes [24]. In such cases, the time-stacked tomograms exhibit a resistivity 'texture' which may act to 'fingerprint' and hence infer certain gross properties such as the state of coalescence. Summary indexes bases on the estimated resistivity distribution, either globally [24] or within suitably defined spatial regions have been developed for analysing heterogeneity in mixing tanks [26] and bubble-columns [27] based on ERT or ECT measurements, respectively. Such analytical tools could readily be extended to treat MERT data.

4. Conclusion

There is a recognised desire for an instrument capable of the rapid characterisation of fine particles, colloids, emulsions and pastes. Ideally, such an instrument would require a minimum of sample preparation and could be used to monitor or control the processing of particulate systems. This has motivated the development and evaluation of small-scale ERT sensors. From the presented material the following conclusions can be made.

Several sensors comprising 16 axially extended electrodes have been constructed and evaluated using phantoms or controlled flow rigs. These can be considered as feasibility studies to determine whether the principles of ERT can be extended to the required small scale. Potential difficulties include the precise manufacture of the sensor, consideration of the high current densities produced and the influence of the close proximity of the electrodes and cabling.

The use of printed circuit technology is attractive, particularly as it permits the signal conditioning measurement electronics to be closely associated with the electrodes. Using PCB technology would lower the unit manufacturing cost so that the sensor could be deployed at several sites along a production plant, or used in application requiring disposable sensors.

As feasibility studies, it is sensible to initially deploy existing DAS and tomographic reconstruction algorithms, hence the widely employed 16 electrodes, adjacent measurement protocol and LBP combination. The axially extended electrode sensors compliment this combination, which explains their relative success, particularly when imaging single rod phantoms.

There is, however, a danger of treating ERT as a 'magic microscope', where potentially widely differing information can be extracted using the same, basic, approach. The path of, particularly pixel based, tomographic reconstruction followed by image feature extraction is inherently ill posed and computationally intensive. This is illustrated by the results of the rod phantom analysis summarised in Table 1. Many of the potential applications of MERT involve monitoring dynamic processes, thus requiring speed in both the data acquisition and also in the data processing.

A better approach would be to first determine which information is required for that *specific* application, and then to integrate the geometry of the sensor transducer array and measurement protocol such that the computation required to extract this information is minimised. Note that this approach may be extended to include multi-modal sensors and subsequent employment of data fusion methods [28].

References

[1] H.S. Tapp, R.H. Wilson, Developments in low-cost electrical imaging techniques, Process Control Quality 9 (1–3) (1997) 7–16.
[2] F. Dickin, M. Wang, Electrical resistance tomography for process applications, Meas. Sci. Technol. 7 (3) (1996) 247–260.
[3] A.J. Peyton, Z.Z. Yu, G. Lyon, S. AlZeibak, J. Ferreira, J. Velez, F. Linhares, A.R. Borges, H.L. Xiong, N.H. Saunders, M.S. Beck, An overview of electromagnetic inductance tomography: description of three different systems, Meas. Sci. Technol. 7 (3) (1996) 261–271.
[4] N. Reinecke, D. Mewes, Recent developments and industrial/research applications of capacitance tomography, Meas. Sci. Technol. 7 (3) (1996) 233–246.
[5] J. Suehiro, R. Pethig, The dielectrophoretic movement and positioning of a biological cell using a three-dimensional grid electrode system, J. Phys D: Appl. Phys. 31 (22) (1998) 3298–3305.
[6] C.E. Hodgson, R. Pethig, Determination of the viability of *Escherichia coli* at the single organism level by electrorotation, Clinical Chem. 44 (9) (1998) 2049–2051.
[7] X.F. Zhou, J.P. Burt, R. Pethig, Automatic cell electrorotation measurements: studies of the biological effects of low-frequency magnetic fields and of heat shock, Phys. Med. Biol. 43 (5) (1998) 1075–1090.
[8] G.H. Markx, R. Pethig, J. Rousselet, The dielectrophoretic levitation of latex beads, with reference to field-flow fractionation, J. Phys D: Appl. Phys. 30 (17) (1997) 2470–2477.
[9] A.D. Goater, J.P.H. Burt, R. Pethig, A combined travelling wave dielectrophoresis and electrorotation device: applied to the concentration and viability determination of *Cryptosporidium*, J. Phys D: Appl. Phys. 30 (18) (1997) L65–L69.
[10] J. Cheng, E.L. Sheldon, L. Wu, A. Uribe, L.O. Gerrue, J. Carrino, M. Heller, J. O'Connell, Electric field controlled preparation and hybridization analysis of DNA/RNA from *E. coli* on microfabricated bioelectronic chips, Nature Biotechnol. 16 (1998) 541–546.
[11] T. York, A. Somerville, I. Evans, A sensing circuit for micro-capacitance tomography, in: Conf. Proc. 1st World congress on industrial process tomography, 14–18 April 1999, Buxton, UK.

[12] M. Wang, F. Dickin, Visualisation of solid/liquid flow in a small-bore pipeline using electrical resistance tomography, Schlumberger Cambridge Research Lab., U205, 1994.
[13] M. Wang, F. Dickin, R. Mann, Electrical resistance tomographic sensing systems for industrial applications, in: Conf. Proc. on frontiers industrial process tomography II, 8–12 April 1997, TU Delft, pp. 179–184.
[14] Industrial Tomography Systems, Fairbairn Building, 72 Sackville Street, PO Box 88, Manchester, M60 1QD.
[15] D.C. Barber, B.H. Brown, Applied potential tomography, J. Phys E: Sci. Instrum. 17 (9) (1984) 723–733.
[16] Z. Abdullah, S. Quick, F.J. Dickin, Quantitative algorithm and computer architecture for real-time image reconstruction in process tomography, in: Tomographic Techniques for Process Design and Operation, Computational Mechanics, Southampton, 1993, pp. 179–192.
[17] R.M. West, X. Jia, R.A. Williams, Parametric modelling in industrial process tomography, in: Conf. Proc. 1st World congress on industrial process tomography, 14–18 April 1999, Buxton, UK.
[18] Ø. Isaksen, A review of reconstruction techniques for capacitance tomography, Meas. Sci. Technol. 7 (3) (1996) 325–337.
[19] Ø. Isaksen, J.E. Nordtvedt, A new reconstruction algorithm for process tomography, Meas. Sci. Technol. 4 (1993) 1464–1475.
[20] Ø. Isaksen, J.E. Nordtvedt, An implicit model based algorithm for use with a capacitance tomography system, in: Process Tomography — a Strategy for Industrial Exploitation — 1994, UMIST, Manchester, 1994, pp. 215–226.
[21] H. Griffiths, M.G. Tucker, J. Sage, W.G. HerrendenHarker, An electrical impedance tomography microscope, Physiol. Meas. 17 (S4A) (1996) A15–A24.
[22] A. Nesbet F.J. Dickin, R.A. Williams, Microelectrical tomography of flowing colloidal dispersions and dynamic interfaces, in: Process Tomography — a Strategy for Industrial Exploitation — 1993, UMIST, Manchester, 1994, pp. 280–283.
[23] R.A. Williams, A. Nesbet, F.J. Dickin, S.E. Taylor, Microelectrical tomography of colloidal systems, Process Tomography — a Strategy for Industrial Exploitation — 1994, UMIST, Manchester, 1994, pp. 15–24.
[24] P. Gregory, R.A. Williams X. Jia, T.M. Shi, S.P. Luke, Characterisation of structured suspensions and emulsions using tomographic electrical texture fingerprinting, in: Conf. Proc. on frontiers industrial process tomography II, 8–12 April 1997, TU Delft, pp. 3–8.
[25] P. Gregory, M. Phil. Transfer Report,University of Exeter, 1996.
[26] J. Bond, I. Faulks, X. Jia, K. Ostrowski, R.M. West, R.A. Williams, Optimisation of solid–liquid mixing using three-dimensional resistance tomography, in: Conf. Proc. on frontiers industrial process tomography II, 8–12 April 1997, TU Delft, pp. 343–348.
[27] M.A. Bennett, S.P. Luke, X. Jia, R.M. West, R.A. Williams, Analysis and flow regime identification of bubble column dynamics, in: Conf. Proc. 1st World congress on industrial process tomography, 14–18 April 1999, Buxton, UK.
[28] R.M. West, R.A. Williams, Opportunities for data fusion in multi-modality tomography, in: Conf. Proc. 1st World congress on industrial process tomography, 14–18 April 1999, Buxton, UK.